BELLCOMM, INC.

TR-65-340-1

Solar Cosmic Ray Events

November 1, 1965

R. H. Hilberg

Work performed for Manned Space Flight, National Aeronautics and Space Administration under Contract NASw-417.

TABLE OF CONTENTS

ABSTRACT

15769

Solar cosmic ray events are felt to present the greatest hazard to the Apollo astronauts of all of the natural radiation sources. This report describes the nature of the charged particle fluxes in the vicinity of the earth in order to analyze the magnitude of the hazard.

The temporal dependence, spectral shape, size and composition of the events of the 19th solar cycle peak (1956-1961) are discussed. Best estimates for these properties are presented for each event, and from these a dose-probability curve is calculated. This is done using distribution functions to summarize the properties of the events.

An effort is made to analyze the accuracy to which the radiation environment has been measured. The detection systems used are described with an estimate of the accuracy as well as the overall advantages and disadvantages of each.

Every effort should be made to reduce the uncertainties of our knowledge of the next peak in solar activity. The ideal program would include continuous monitoring outside of the magnetosphere of the particle flux, spectra, time dependence, and composition.

Author

SOLAR COSMIC RAY EVENTS

I. Introduction

This report will present a description of the solar cosmic ray environment, with emphasis placed on developing an estimate of the uncertainty in the estimated hazard to the Apollo astronauts. Since our understanding of the environment is the result of various measuring devices, the merits and limitations of the instruments used in obtaining cosmic ray data will be analyzed. A useful method of applying the observed environment to describe the radiation hazard to the astronauts will be presented. The intention here is to emphasize basic aspects of the analysis of solar cosmic ray data rather than to present new or better data.

Solar cosmic ray events have been singled out from other sources of radiation because they are felt to present the greatest hazard to Apollo. The events of interest are those which produce high fluxes (of the order of 10^8 protons/cm^2 or more) with energies in the 1 Mev to 1 Bev range in the vicinity of the earth, lasting for several days. The characteristic of these events which is largely responsible for the hazard to Apollo is the fact that they occur randomly in time and cannot as yet be forecast in advance. The part of the energy spectrum of interest to the Apollo program is that between 30 Mev and 100 Mev. This is because protons with less than 30 Mev cannot penetrate the thinnest parts of the Command Module, while those with more than 100 Mev are much less numerous than those in the 30 to 100 Mev range. Protons with less than 30 Mev can penetrate the Lunar Excursion Module and the spacesuit, so they cannot be neglected for portions of the mission when some of the astronauts are outside the CM.

In short, the problems to be discussed in this report are:

(1) What do we know about the solar cosmic ray environment? How do we know it? How well do we know it?

(2) What do we want to know?

(3) How can the interaction of the cosmic ray environment with the Apollo astronauts be best analyzed?

2. Observations of Solar Cosmic Rays

In this section the techniques used to measure solar cosmic ray intensities, spectra, and composition as functions of time will be described. The experimental uncertainties of the obtained values will be estimated.

There was no extended period of the 19th Solar Cycle (1956-1961) during which complete coverage of the cosmic ray environment was attained. All ground based observations required detailed theoretical analysis to convert observed data to primary cosmic ray fluxes in the energy range of interest. This analysis was too complicated to give confidence in the results. In-flight observations were not complete, with the times of peak flux occasionally missed.

2.1 Polar Cap Absorption Measurements

When energetic cosmic rays enter the atmosphere, they lose energy by ionizing the air molecules. As the density of ionization increases, the ability of radio waves to traverse the medium decreases and the waves are absorbed.

The three most successful systems which have been developed to observe this phenomenon are the Riometer, the V.H.F. ionospheric scatter network, and the F min system. The Relative Ionospheric Opacity Meter (Riometer) measures the ionospheric absorption of cosmic radio noise.[1] The V.H.F. ionospheric scatter network transmits a radio wave from one station and observes the wave after reflection from the ionosphere at a second station about 1000 Km to 2000 Km away.[2] F min systems measure the minimum frequency of radio waves that can be transmitted vertically, with the echo from the ionosphere received on earth.[2,3]

The theory which relates the absorption of radio waves by the ionosphere to the incident flux of cosmic rays is presented by Leinbach.[1] The radio absorption depends on the density of ionization-altitude profile, which in turn depends on the spectral shape and intensity of the incident cosmic rays. Calculations indicate that the observed absorption does not depend strongly on the spectral shape.[4,5] Thus, only integral intensity values above a cutoff energy can be expected.

The fact that most of the absorption is expected to occur at an altitude of 50-100 Km implies a minimum, atmospheric, cutoff energy of about 10 Mev. In addition, because of the earth's magnetic field, only particles above a particular cutoff rigidity can reach a given observer[11,14] with the value of the cutoff rigidity depending primarily on the magnetic latitude. Rigidity is defined by equation 3-4. The intensity of cosmic rays measured is thus the integral flux above the corresponding cutoff energy. Since the earth's magnetic field changes in magnetic storms, the value of the cutoff energy or the radio absorption may change during parts of the cosmic ray events.

Since the experimental accuracy is about the same for all PCA observations and the interpretive assumptions are similar, only Riometer data will be discussed here. The Riometer data is uncertain by about $\pm 20\%$ in the calculated absorption.[15] In addition to the purely experimental limitations, there is about a factor of 2 uncertainty in the interpretation of the data.[6]*

2.2 Neutron Monitors

Because of the dense atmosphere, very few cosmic rays reach the earth. However, many energetic (E>1 Bev) ones produce neutrons which can penetrate the atmosphere and be detected by earth based neutron monitors. Energetic solar cosmic rays and galactic cosmic rays both produce such neutrons, so that galactic cosmic rays produce a background counting rate which sets a lower limit on the solar cosmic ray fluxes observable with this type of monitor. Therefore, solar cosmic ray fluxes with few particles in the Bev range will not be seen.

Observations made at several stations located at different geomagnetic latitudes can yield integral fluxes above several energies. These integral fluxes can be combined to give information on the spectral shape of the particle fluxes in the Bev energy region.

The accuracy of the cosmic ray fluxes deduced from the neutron monitor is limited primarily by the considerations used in the interpretation. The yield depends to some extent on the spectral shape which is unknown unless spectral data from other

---

*This factor of 2 represents the expected error in the resulting flux value.

monitor stations or satellite observations are available. It is estimated in the Solar Proton Manual[6] that cosmic ray intensities are uncertain by up to a factor of two.

As indicated above, neutron monitors observe effects produced by particles in the Bev energy range. Extrapolation to the region of primary interest (30 Mev to 100 Mev) is questionable, so that these measurements are not as valuable as lower energy measurements. However, the monitoring is continuous and the resulting checks on other measurements are helpful.

2.3 Primary Particle Detectors

Because of the earth's atmosphere, primary cosmic rays can be detected only by in-flight detectors. The flight systems used in the 19th solar cycle were balloons, rockets, and satellites.

Balloons have the limitation that they cannot escape the atmosphere completely, but the experiments use this fact to advantage by using the residual atmosphere above the balloon as an absorber and measuring integral fluxes. Spectral shapes can be measured by observing integral fluxes during the ascent of the balloon through the atmosphere.

Rockets containing detectors have been launched when another system, such as the riometer, observed the presence of solar cosmic rays. With such a flight system observers can combine the advantage of continuous monitoring of the ground based system with the increased data capabilities of in-flight measurements.

Satellites offer the best coverage for monitoring in the range of interest. The detectors can be selected from considerations of the quantities to be measured with fewer restrictions set by the in-flight system.

Geiger counters detect only the passage of particles through the Geiger tube and give no information on the energy or specific energy loss. The specific energy loss of a particle is defined as $-\frac{dE}{dx}$ (Mev-cm^2/gm) which is the energy deposited by a particle per gram/cm^2 of material traversed. The range R of an energetic proton is defined by:

$$R(E) = \int_E^0 \frac{dE}{\left(\frac{dE}{dx}\right)}$$

where E is the initial energy of the particle. There is a 1:1 correspondence between the energy of a particle and its range in a given material. Energy information can be obtained with a Geiger tube by observing the flux of protons traversing a given absorber, since all such protons have initial ranges greater than the thickness of the absorber.

Ionization chambers count the total ionization of particles passing through the counter. Usually an ionization chamber measures "specific ionization". The fact that galactic cosmic rays have lower specific ionization than solar cosmic rays enables the ionization chamber to discriminate against galactic cosmic rays better than the geiger counter. The combination of ionization chamber, geiger counter, and absorber enables one to obtain information on spectrum and composition.

Scintillators with photomultiplier tubes and silicon junction detectors have also been used to detect cosmic rays. Both types measure the energy of the particle detected. Nuclear emulsions have also been used. Emulsions give time integrated energy and composition information but no information on temporal dependence.

Except for the Geiger tubes, all of these detectors have sufficient resolving power so that very little uncertainty is introduced in measuring an integral energy spectrum by limitations in detector resolution. Relatively high uncertainties are introduced by geometrical and efficiency considerations. While the efficiency of each of these detectors in detecting energetic protons and alpha particles is 100% under ideal conditions, statistical requirements combined with relatively low counting rates necessitate non-ideal configurations. For example, rather than use a thin scintillator on the surface of a photomultiplier with good light collection, a large crystal with poor light collection may be necessary. On such large detectors the efficiency is difficult to calculate or measure. Complicated configurations of absorbers and detectors combine with environmental conditions, such as trapped radiation and the earth's magnetic field, to restrict the accuracy of flux measurements. W. Webber estimates an error of about $\pm$25% for in-flight flux measurements.(3)

Table 1 summarizes the energy regions measured in the 19th solar cycle with the detection techniques used for each. It is noted that satellite data extend back only to 1960. Since balloons and rockets usually were launched after the arrival at earth of cosmic rays, the data is more useful in giving spectral shape than for time integrated fluxes.

Satellite data is superior to ground based and other in-flight data because it provides direct measurement of the particle fluxes throughout each event. However, better coverage could be obtained by means of a satellite which was outside of the magnetosphere a higher fraction of the time, ideally, all of the time.

3. Characteristics of the 19th Solar Cycle Events

In this section the solar cosmic ray events of the 19th solar cycle will be described in some detail. The properties of the events will be discussed in an attempt to evaluate a standard format to which the majority of the events conform. Table 3 presents current best values for parameters used to describe the temporal dependence, the size,and the composition of each of the events of the 19th solar cycle. The significance of the parameters listed is described in this section. In order to make these quantities meaningful, the bulk of this section is given to a description of the phenomenology of the events as far as the near-earth region is concerned.

The forms in which the events are usually described will be presented and a table of the parameters applicable for each event (Table 3), will be included. It is not true that all events can best be described by the standard format, but it is desirable, from the point of view of analysis, to use a single representation.

3.1 Temporal Dependence

There are three characteristic times describing each cosmic ray event: the onset-delay time, the rise time, and the decay time. These quantities are shown in Figure 1. It should be noted that these quantities are different for each energy range considered.

It has become conventional to describe the temporal dependence of particle flux by exponential expressions:

$$J = J_p \exp\left(\frac{t-t_p}{t_R}\right) \qquad o < t \leq t_p \qquad (3\text{-}1)$$

$$J = J_p \exp\left(-\frac{t-t_p}{t_D}\right) \qquad t_p \leq t \qquad (3\text{-}2)$$

where J is the instantaneous particle flux rate, J_p is the peak particle flux rate, t_p is the time of peak flux, t_R is the rise time, and t_D is the decay time. To this approximation the time integrated particle flux is

$$N = \int_0^\infty J \, dt = J_p \, (t_R + t_D) \qquad (3\text{-}3)$$

Reference 6 presents the time dependence of most events. It can be seen that parts of most events can be described by such equations, but very few events can be described well during most of their duration by a single set of parameters. However, the values listed in Table 3 are useful in that they give a rough estimate of the duration of each event. While equations 3-1 and 3-2 are usually used to describe the temporal dependence of the flux intensity, they cannot be considered accurate representations but mere conveniences.

3.2 Spectral Shape

It has been found[7] that many cosmic ray events can best be described in terms of an exponential rigidity spectrum. A detailed discussion of this description, including examples, is found in Reference (7). The rigidity of a charged particle is defined as:

$$R = \frac{pc}{eZ} \qquad (3\text{-}4)$$

where p is the particle's momentum in Mev/c, c the velocity of light, e the absolute value of the charge of the electron in electrostatic units, and Z the atomic charge of the particle. Thus, the number of particles with rigidity greater than R is given by

$$N(>R) = N_o e^{-R/R_o} \qquad (3\text{-}5)$$

where R_o is the characteristic rigidity of the event and is defined by the above equation. The units of R are volts. A table relating energy to rigidity for protons, alpha particles, and electrons is given by McKee and Bohlin.[8]

Figure 2 gives the distribution of the observed values of characteristic rigidities for the events of the 19th solar cycle containing a total flux of 10^6 protons/cm^2 or more with energies greater than 30 Mev. $n(>R_o)$ represents the number of events having characteristic rigidity greater than R_o. The large uncertainties in the values prevent a unique choice of distribution functions from being chosen. Both the linear distribution

$$\int_{R_o}^{\infty} h(R_o)dR_o = \begin{cases} 1 & ; R_o < 40 \text{ Mv} \\ 1.3 - .0095\, R_o & ; 40 \text{ Mv} < R_o \leq 145 \text{ Mv} \\ 0 & ; 145 \text{ Mv} < R_o \end{cases} \qquad (3\text{-}6)$$

and the exponential function

$$\int_{R_o}^{\infty} h(R_o)dR_o = e^{-R_o/52} \qquad (3\text{-}7)$$

fit the observed distribution to within experimental uncertainty. Both of these expressions fulfill the normalization requirement.

$$\int_{o}^{\infty} h(R_o)dR_o = 1 \qquad (3\text{-}8)$$

The advantage of the exponential rigidity spectrum description of an event is that a single parameter accurately describes the particle spectrum over wide ranges of rigidity or energy. This suggests that such a description may be basic to the acceleration and propagation process. However, the characteristic rigidity is not necessarily constant over an entire event. If the rigidity changes during an event, the time integrated spectrum may not be as accurately exponential as the instantaneous spectrum. Of the events considered in Reference 7, only about 30% had constant rigidity, with the characteristic rigidity

decreasing with time during the course of the other events. Since the rigidity was fairly constant during the times of peak flux, the time integrated spectrum was reasonably well described by an exponential distribution in most cases.

3.3 Composition

Data on the composition of solar cosmic rays is limited, being available for only about 25% of the events of the 19th solar cycle. While the composition of solar cosmic rays varies from one event to another, there is a tendency for protons and alpha particles to be about equally abundant, with heavier ions much less significant. Table 2 is taken from Schulte[9] and gives relative fluxes of various positive ions based on data taken from the September 3, November 12 and November 15, 1960 events.[10] About 60% of the events observed contained proton/alpha particle ratios consistent with the above assumption, while only a few events were greatly at variance with it. For purposes of analysis such a model is useful. The ratio of proton flux to alpha particle flux is given in Table 3 for the events in which data is available.

3.4 Particle Fluxes

The integral cosmic ray fluxes are usually presented in terms of the total number of protons with rigidities greater than R integrated over the time of the whole event, for R values of 137 Mv, 239 Mv, and 445 Mv (1 Mv = 10^6 v) corresponding to energies of 10 Mev, 30 Mev and 100 Mev, respectively. In several cases, when several events originated from the same spot on the sun and were separated by only a few days, they were treated as a single event in one curve in Figure 3. Such events which were close to each other in both time of occurrence and in position on the sun were considered to be a single solar event. The flux values are the same as given in Table 3. The probability values were obtained by assuming random time distribution during the 6 years of solar maximum, 1956-1961.

The event size distribution for the ungrouped events can be described with fair accuracy by the expression:

$$\int_N^\infty g(N(>30))\, dN(>30) = \begin{cases} .0476 - .00511 \log_{10}\left[N(>30)\right]; N \leq 2\times10^9 \ \frac{\text{protons}}{\text{cm}^2} \\ 0 \qquad\qquad\qquad\qquad ; N > 2\times10^9 \ \frac{\text{protons}}{\text{cm}^2} \end{cases} \tag{3-9}$$

$\int_{N(>30)}^{\infty} g(N'(>30))dN'(>30)$ is the fraction of days in the 6 year maximum of the 19th solar cycle in which an event of size N(>30) or larger occurred.

The peak intensity, J(>R), is given by

$$J(>R) = \frac{N(>R)}{t_R(R) + t_D(R)} \qquad (3\text{-}10)$$

to the extent that the exponential representation of the time dependence is correct.

Table 3 presents some significant parameters for the events of the 19th solar cycle. Values are taken from References 3 6 and 7 although most of them have been checked with calculations made from published data. The experimental uncertainties can be estimated from the values given in Table 1.

The first two columns give values for the onset plus rise time, expressed in hours, for protons above two energy levels. The next two columns contain decay times. Numbers given in parentheses are estimated values.

The next three columns contain total fluxes with energies above each of three values, integrated over the entire event. These fluxes are given in units of protons/cm^2.

The characteristic rigidities given are calculated from the equation

$$R_o = \frac{206}{\ln\left[\frac{N(>30\ \text{Mev})}{N(>100\ \text{Mev})}\right]} \qquad (3\text{-}11)$$

which results simply by assuming that the spectrum is accurately exponential in rigidity above 30 Mev. The data from 30 Mev to 100 Mev is used without regard to the flux above 10 Mev.

The errors assigned to the values in Figure 3 are based on error estimates summarized in Table 1. The rigidity values required two flux measurements (e.g., N(>30 Mev) and N(>100 Mev)), and the error is propagated appropriately, using equation 3-11 as a definition.

The ratios of proton fluxes to alpha particle fluxes are based on fluxes per equal rigidity interval. It has been observed for some events that the same R_o describes α and proton spectra.[7,9] If this is generally true, then the ratio of proton to alpha particle fluxes should be independent of the rigidity range observed.

4. Applications

It is useful to use the empirical distribution functions presented in Section 3 in calculating a dose probability curve for the Command Module. The calculation which will be done is for a specific case,and the purpose of the calculation is to illustrate the use of the distribution functions.

The quantity to be evaluated is

$f(D)dD$ = the probability per day of being exposed to a dose between D and D+dD

The first assumption made is that the dose is a function of N(>30) and the characteristic rigidity only, for a given shielding configuration:

$$D = D(N[>30],R_o) \qquad (4\text{-}1)$$

and that any one of these quantities can be expressed in terms of the other two.

$F(N[>30],R_o)\ dR_o dN[>30]$ represents the number of events with characteristic rigidities between R_o and R_o+dR_o and flux between N[>30] and N[>30] + dN[>30]. For convenience, the symbol N will be used to represent N[>30] in the following:

$$f(D)dD = \int' F(N,R_o)dR_o dN \qquad (4\text{-}2)$$

The prime on the integration indicates that only values of N and R_o related by equation 4-1 are included in the summation.

The next simplifying assumption that will be made is that N is independent of R_o, so that

$$F(N,R_o) = g(N)h(R_o) \qquad (4\text{-}3)$$

The events of the 19th solar cycle are plotted as a function of N[> 30 Mev] and R_o in Figure 5. While the points do not seem purely random, there is no 1:1 relationship between N[> 30 Mev] and R_o, and the assumption of a random scatter should introduce only a small error in the results.

Substituting equation 4-3 into 4-2:

$$f(D)dD = \int' g(N)\, h(R_o)\, dR_o dN \qquad (4-4)$$

$$= \int g(N[D,R_o])\, h(R_o)\, \frac{\partial(R_o,N)}{\partial(R_o,D)}\, dR_o\, dD$$

$$= \int g(N[D,R_o])\, h(R_o)\, \frac{\partial N}{\partial D}\, dR_o\, dD \qquad (4-5)$$

or

$$f(D) = \int_0^\infty \frac{\partial N}{\partial D}\, g(N)\, h(R_o)\, dR_o \qquad (4-6)$$

$\frac{\partial(R_o N)}{\partial(R_o D)}$ is the Jacobian of the transformation from R_o,N coordinates to R_o, D coordinates.

It should be noted that g(N), f(D), and $F(N,R_o)$ are defined as probabilities per day, while $h(R_o)$ is normalized to unity.

A calculation by E. N. Shipley[12] indicated that the Command Module dose per proton or alpha particle depends on the characteristic rigidity in the manner shown in Figure 4. Since many solar cosmic ray events seem to have equal fluxes of protons and alpha particles per rigidity interval, this equality can be taken as universal for the purposes of the present analysis. For this case, Figure 4 indicates that the expression

$$D(N[>30\ \text{Mev}],R_o) = 0.45 \times 10^{-9}\ N[>30\ \text{Mev}]\ R_o \qquad (4-7)$$

empirically describes the dose given by an event of the size given by N and a spectral shape described by R_o. This expression is valid at the center of the capsule for this particle composition using the particular shielding described in Ref. 12. The simplicity of (4-7) is fortuitous, as is suggested by the three curves of Figure 4.

Equation (3-9) states that

$$\int_N^\infty g(N(>30))\, d\,N(>30) = \begin{cases} .0476 - .00511 \log_{10}[N(>30)]; & N \leq 2 \times 10^9 \ \frac{\text{protons}}{\text{cm}^2} \\ 0; & 2 \times 10^9 < N \end{cases} \qquad (4\text{-}8)$$

which yields:

$$g(N(>30)) = \begin{cases} .00221/N \ ; & N \leq 2 \times 10^9 \ \frac{\text{protons}}{\text{cm}^2} \\ 0 \ ; & 2 \times 10^9 \ \frac{\text{protons}}{\text{cm}^2} < N \end{cases} \qquad (4\text{-}9)$$

From equation (3-6):

$$\int_{R_o}^\infty h(R_o)dR_o = \begin{cases} 1 & ; \ R_o < 40 \text{ Mv} \\ 1.3 - .0095\, R_o & ; \ 40 \leq R_o \leq 145 \text{ Mv} \\ 0 & ; \ 145 < R_o \end{cases} \qquad (4\text{-}10)$$

which yields:

$$h(R_o) = \begin{cases} 0 & ; \ R_o < 40 \text{ Mv} \\ .0095 & ; \ 40 \leq R_o \leq 145 \text{ Mv} \\ 0 & ; \ 145 < R_o \end{cases} \qquad (4\text{-}11)$$

When equation (4-7) is solved for N, one has:

$$N = \frac{D}{.45 \times 10^{-9} R_o} \qquad (4\text{-}12)$$

Substituting equations 4-9, 4-11, and 4-12 into 4-6 and integrating, we have

$$f(D) = \begin{cases} \dfrac{2.2 \times 10^{-3}}{D} & ;D \leq 36 \text{ rad.} \\ \dfrac{2.1 \times 10^{-5}}{D}\,(145 - D/.9) & ;36 \text{ rad} \leq D < 131 \text{ rad.} \\ 0 & ;D > 131 \text{ rad.} \end{cases} \quad (4\text{-}13)$$

$$\int_D^\infty f(D)dD = \begin{cases} .010 - .005 \log_{10} D & ; \quad D < 36 \text{ rad.} \\ .012 - .007 \log_{10} D + 2.3 \times 10^{-5} D & ;36 \leq D \leq 131 \\ 0 & ; \quad 131 < D \end{cases} \quad (4\text{-}14)$$

This distribution function is shown in Figure 6 along with Shipley's calculated dose points.

An interesting aspect of the dependence of the dose distribution on $h(R_o)$ can be seen by considering

$$f(D) = \int_o^\infty \frac{\partial N(D,R_o)}{\partial D}\; g(N[D,R_o])\; h(R_o)dR_o \quad (4\text{-}15)$$

In general this is a complicated function of $N(D,R_o)$ $g(N)$, and $h(R_o)$. For the reasonable case (see (4.9))

$$g(N) = \frac{\lambda}{N};0 < N < \infty \quad (4\text{-}16)$$

we have:

$$f(D) = \int_o^\infty \frac{\partial N(D,R_o)}{\partial D}\; \frac{\lambda}{N(D,R_o)}\; h(R_o)\; dR_o \quad (4\text{-}17)$$

which depends on $N(D,R_o)$ and $h(R_o)$. If we now assume

$$N(D,R_o) = m(D)n(R_o) \quad (4\text{-}18)$$

$$f(D) = \int_o^\infty \frac{dm(D)}{dD}\; \frac{\lambda}{m(D)}\; h(R_o)dR_o$$

$$= \frac{\lambda}{m}\; \frac{dm(D)}{dD} \quad (4\text{-}19)$$

because of the normalization requirement of $h(R_0)$ (equation 3-8). Thus, for the case where equations 4-16 and 4-18 hold, the dose distribution is independent of the rigidity distribution, and a single typical rigidity value can be assumed to apply to all events in calculating a dose distribution. The particular rigidity value chosen affects the normalization and, therefore, the maximum possible dose, but does not affect the shape of the distribution. The generality of this result is limited by the finite range of validity of 4-6 in the real case, which results in an overestimate of the dose probability in the regions of these limits.

The analysis of the distribution of doses for the events of the 19th solar cycle by the present method does not introduce significant new information but is intended to demonstrate the use of this approach. Dose is not a basic quantity, especially when an arbitrary shield such as the command module is introduced. A basic theory of cosmic ray events should be able to reproduce the distribution functions.

While no events have been observed giving a dose in the range of 200 rads, an extrapolation can reasonably be made using above considerations. Such extrapolations can be verified only by extensive additional data. However, extrapolations are often necessary, and the above method may well give more reliable results than previous analyses.

There is no guarantee that the events of the 20th solar cycle will be similar to those of the 19th. Therefore, it is important that spectral, intensity, and composition data be obtained as early in the 20th solar cycle as possible. This would mean continuous monitoring, using all systems that were used in the last solar cycle, as well as any improvements now available.

5. Conclusions and Recommendations

While considerable effort has gone into experiments measuring solar cosmic ray properties, the accuracy of the results is still not as high as is needed for a reliable picture of the overall phenomenon. The number of events occurring in a given solar cycle is relatively small so that statistics are poor, and direct measurements were made on a regular basis only late in the cycle.

Another quantity affecting charged cosmic rays is the earth's magnetic field. The problem of estimating the equivalent free space acceptance solid angle of a detector in low earth orbit is extremely complicated, even in times

of magnetic calm. Therefore, it should be helpful to make flux measurements outside of the earth's magnetosphere, on as continuous a basis as possible.

An ideal experimental program concerning the solar cosmic ray environment would include full time monitoring (outside of the magnetosphere) of particle flux, spectra, and time dependence of each type of particle present, and the relative abundances of each type. Such information would enable a more reliable environmental model to be developed.

1011-RHH-gdr

R. H. Hilberg

BIBLIOGRAPHY

(1) H. Leinbach, "Interpretations of the Time Variations of Polar Cap Absorption Associated with Solar Cosmic Ray Bombardments", Geophysical Institute of the University of Alaska, Scientific Report No. 3(May 1962).

(2) D. K. Bailey, "Polar Cap Absorption", Planetary Space Science 12 pp 495-541 (1964).

(3) W. R. Webber, "An Evaluation of the Radiation Hazard Due to Solar Particle Events", Boeing Co. Report D2-90469, (December 1963).

(4) R. R. Brown and R. A. Weir, "Ionospheric Effects of Solar Protons", Arkiv furGeofysik 3, pp 523-529, (1961).

(5) D. K. Bailey, "Abnormal Ionization in the Lower Ionosphere Associated with Cosmic Ray Flux Enhancements", Proceedings IRE, 47 (2), pp 255-266 (February 1959).

(6) F. McDonald, ed. "Solar Proton Manual", NASA TR R-169 (1963).

(7) Freier & Webber, JGR 68 (6), p 1605 (March 1963).

(8) McKee & Bohlin, SUI Report, SUI-63-22.

(9) H. J. Schulte, "Models for Space Environmental Hazards; Radiation", Bellcomm Report, Issue II, January 31, 1964.

(10) S. Biswas, et al, JGR 68, p 3109 (1962).

(11) M. S. Vallarta, Handbuch für Physik 46 (1), p 88 (1961).

(12) E. N. Shipley, Bellcomm Technical Memorandum, TM-64-1012-2 (July 15, 1964).

(13) NASA Publication MDE 8020.008B SE015-001-1, p 39 (1965).

(14) J. J. Quenby & W. R. Webber; Phil. Mag. 4 p 90 (1959).

(15) H. Leinbach; Op. cit. p 61

(16) NASA Technical NOTE TN D-1061 and TN D-1139

(17) K. W. Ogilvie et al, J.G.R. 67 (3) p 929 (March, 1962).

(18) J. F. Steljies & H. Carmichael, J.G.R. 66 (5) p 1363 (May 1961).

(19) B. Maehlum et al, State University of Iowa Report - SUI 62-7 (1962).

(20) C. G. Little & H. Leinbach, Proc IRE 46 p 335 (Jan., 1958).

(21) P. Moyer, et al, P.R. 104, p 768 (1956).

(22) D. Reitz, NASA Reproduction N 63 - 19183 (1963).

(23) K. A. Anderson, et al, J.G.R. 64 (9), pp 1133-1147 Sept, 1959.

(24) J. R. Winkler & P. D. Bhanvar, J.G.R. 65 (9), pp 2637-2655 (1960).

(25) J. R. Winkler, et al, J.G.R. 66 (4) pp 995-1022 (1961).

(26) Anderson & Enemark, J.G.R. 65 (9) p 2657 (1960).

(27) McCracken & Palmeira, J.G.R. 65 (9), p 2673 (Sept, 1960).

(28) W. C. Lin, SUI-61-16 or W. C. Lin and J. A. Van Allen SUI 63-15.

(29) J. R. Winkler, et al, J.G.R. 66 (4) p 1023 (1961).

(30) K. G. McCracken, J.G.R. 67 (2) p 435 (1962).

(31) S. Biswas & P. S. Freier, J.G.R. 66 (4) p 1029 (1961).

(32) S. Biswas, et al J.G.R. 67 (1) p 13 (1962).

(33) J. R. Winkler, et al P.R.L. 6 (9) p 488 (May 1, 1961).

(34) L. R. Davis, et al P.R.L. 6 (9) p 492 (May 1, 1961).

(35) J. G. Roederer, et al P.R.L. 66 p 1603 (1961).

(36) Lockwood & Shea, J.G.R. 66 (10) p 3083 (1961).

APPENDIX

The "Natural Environment and Physical Standards for the Apollo Program" Solar Cosmic Ray Environment

The "Natural Environment and Physical Standards for the Apollo Program" M-D E 8020.008B (SE-015-001-1), April 1965, contains a model representing the expected solar cosmic ray environment. The description includes some collective properties of the events and a specific, more detailed account of a typical event. The model is presented as a basis for design and engineering specifications.

The NEPSAP "model" represents a standard established for the various contributors to the Apollo Program. It gives a complete description of the spectra, intensity, composition, and temporal dependence of solar cosmic ray events with which radiation induced quantities can be calculated. The fact that parts of the description have not been verified experimentally has not been emphasized since it is not relevant to the establishment of the standard. Similarly, estimates of the accuracy of the model are not presented.

The NEPSAP model is derived from the same data that was used in this report, so that the two descriptions are generally consistent. However, since the variation of event parameters from one event to another is considerable, the event described in NEPSAP will be consistent with values observed for very few individual events. For instance, the temporal dependence displayed gives a t_R (>30Mev) $\doteq$ 20 hours and t_R (>100 Mev) $\doteq$ 15 hours. These values are representative of about 30% of the events. The expression relating peak flux to time integrated flux (peak flux = 6×10^{-6} x time integrated flux) and the time dependence curves require a decay time of the order of one day, which is the average decay time of all events. However, 50% of the events had decay times differing from this by over eight hours.

As a standard, the description given in NEPSAP is an adequate representation of the solar cosmic ray environment. It is sufficiently complete that it allows extensive calculations to be made of any of the radiation effects resulting from solar cosmic ray events. It is sufficiently accurate that the results of calculations can be relied on to the extent that a factor of about 2 in the radiation exposure is unimportant.

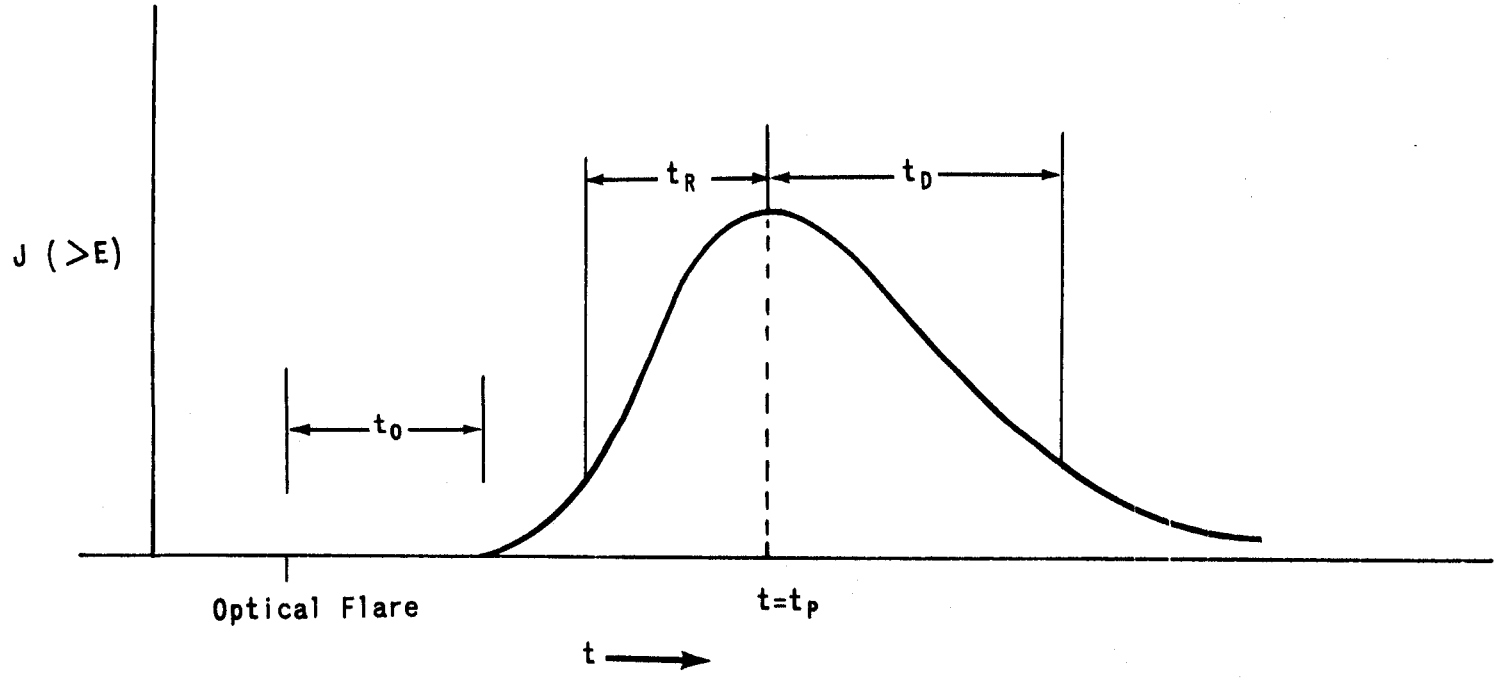

FIGURE 1 TIME DEPENDENCE OF PARTICLE FLUX

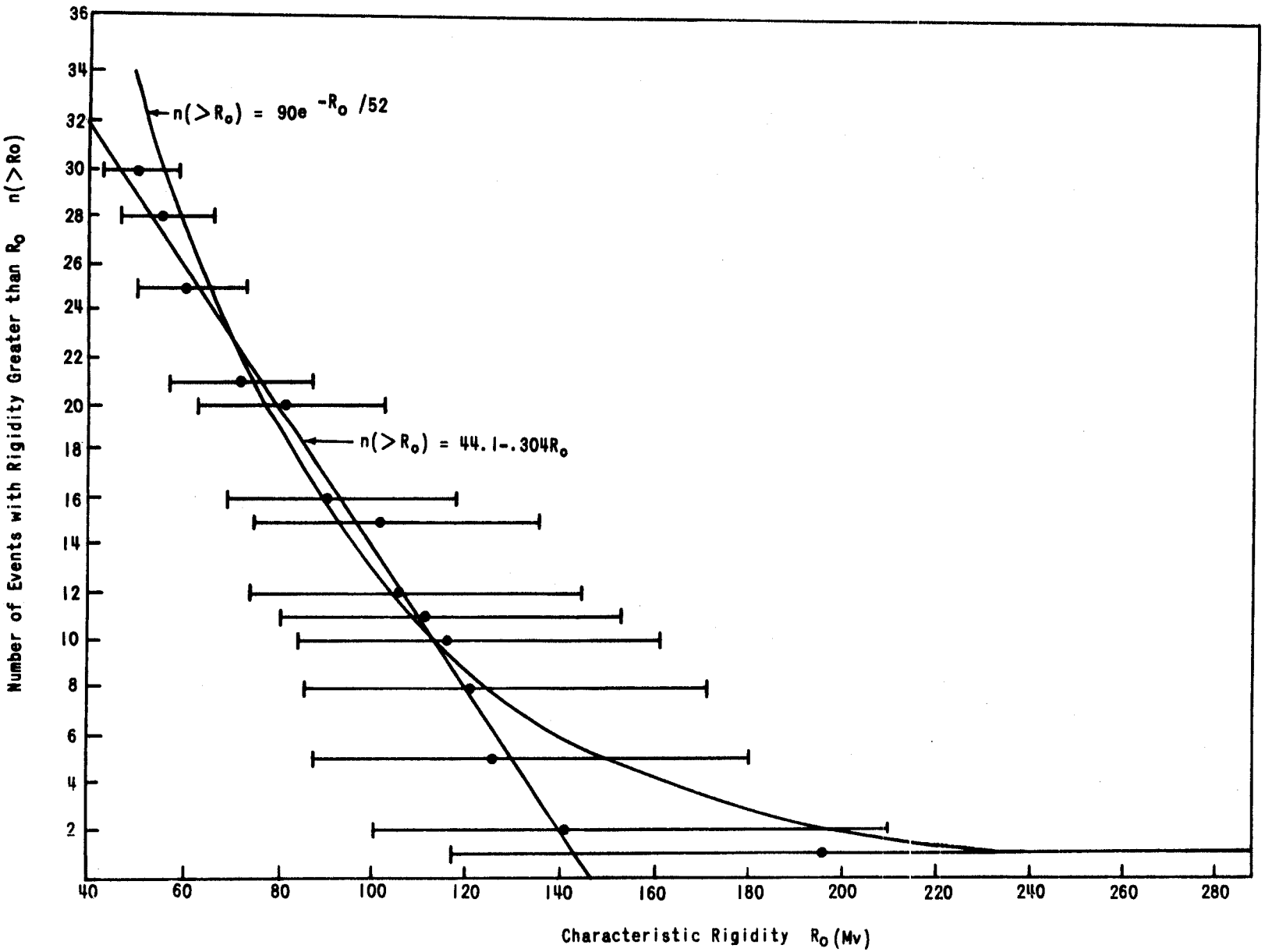

FIGURE 2 DISTRIBUTION OF CHARACTERISTIC RIGIDITY

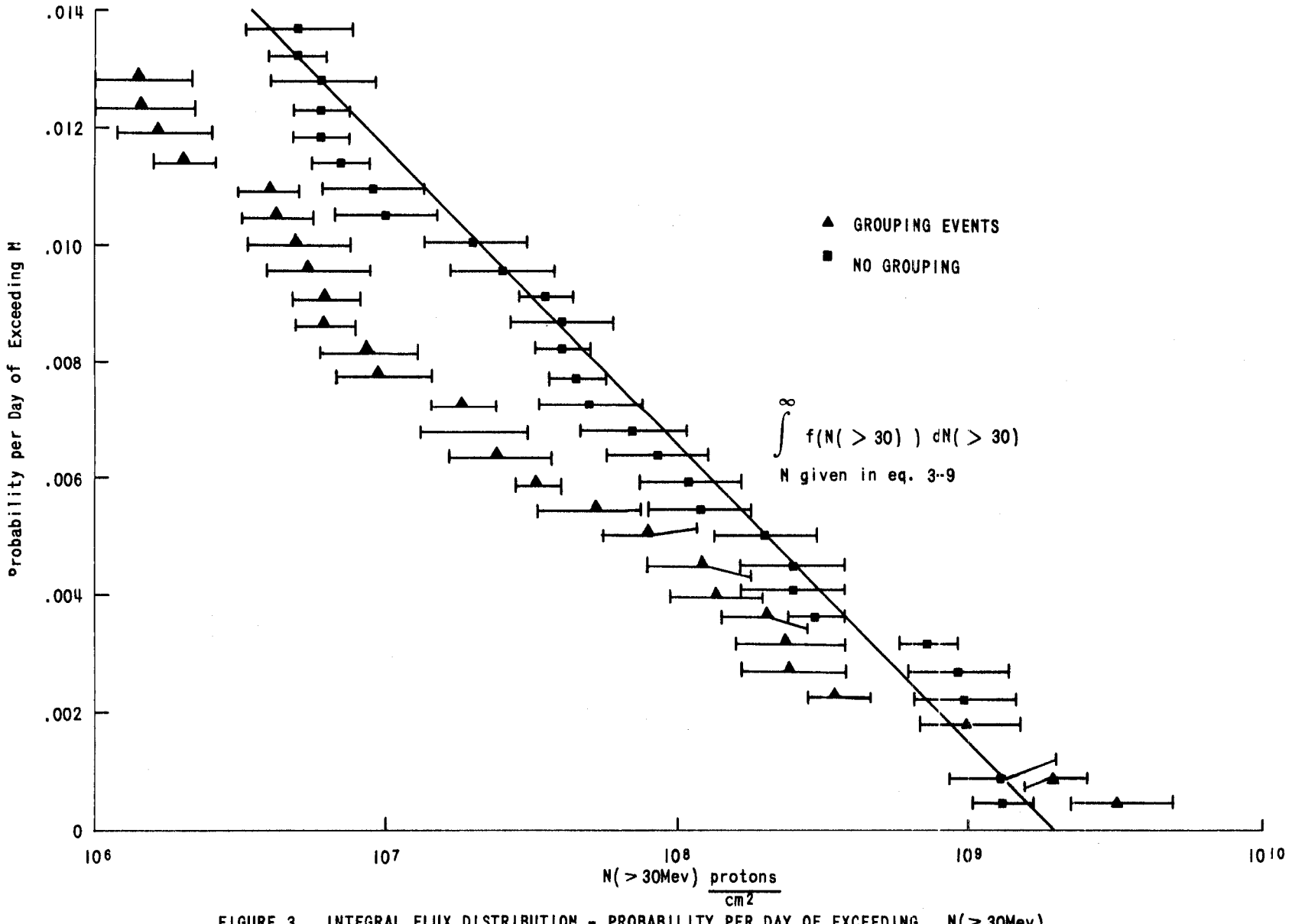

FIGURE 3 INTEGRAL FLUX DISTRIBUTION - PROBABILITY PER DAY OF EXCEEDING N(>30Mev)

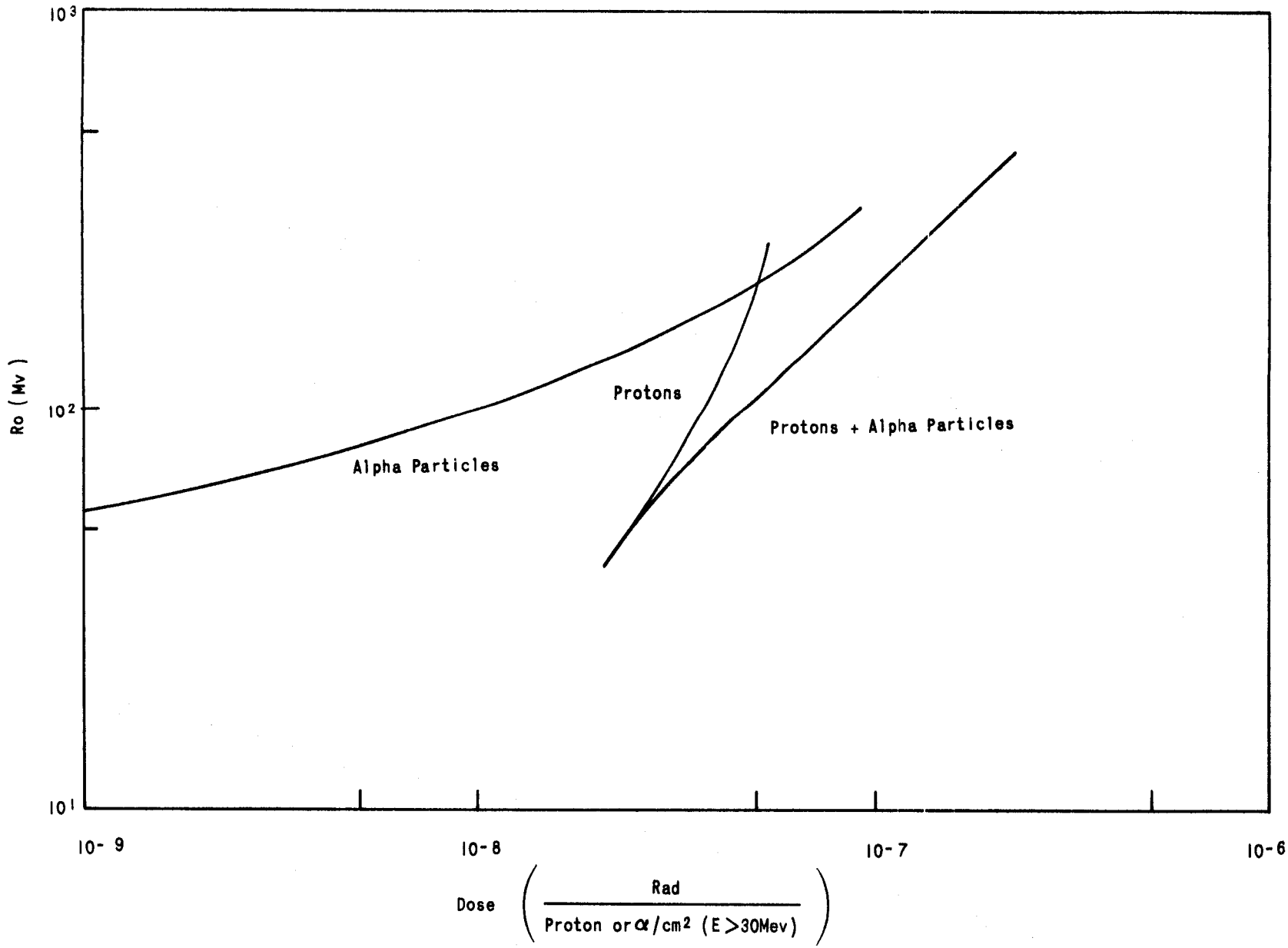

FIGURE 4 EFFICIENCY OF PRODUCING DOSE OF DIFFERENT PARTICLE SPECTRA

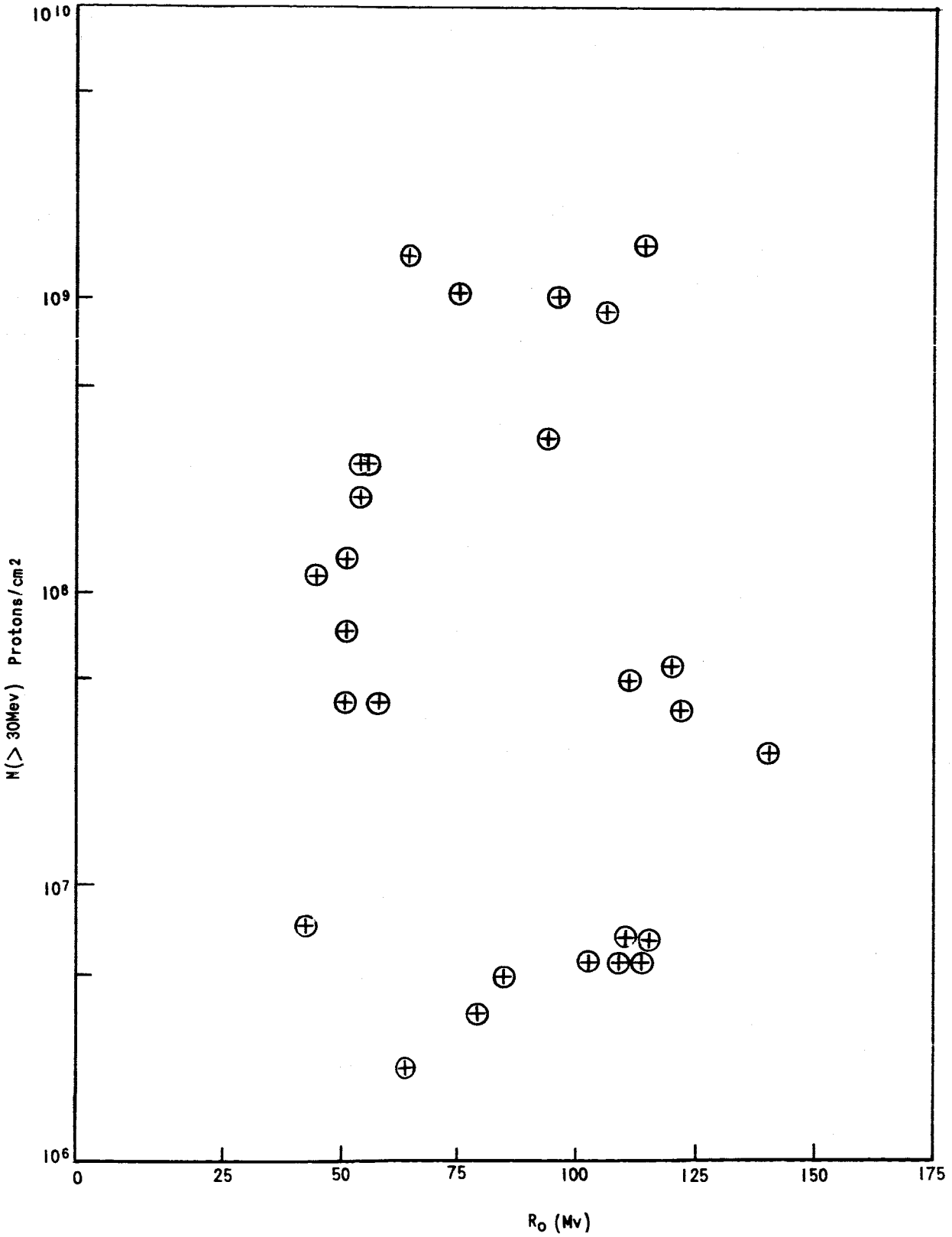

FIGURE 5 CORRELATIONS BETWEEN EVENT SIZE AND R_o

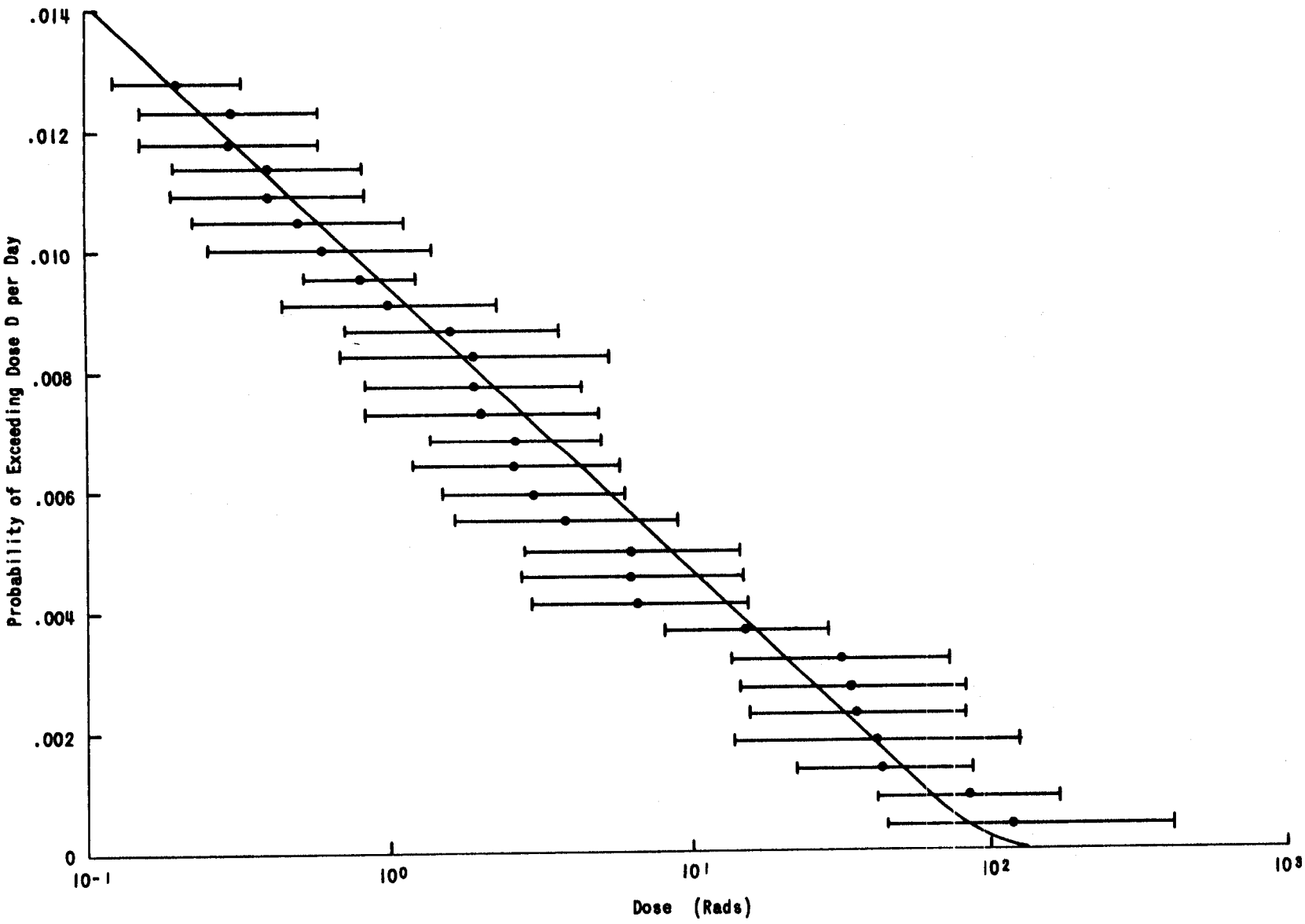

FIGURE 6 COMPARISON OF DOSE PROBABILITY CURVE PREDICTED FROM DISTRIBUTION FUNCTIONS WITH DOSE ESTIMATES FROM INDIVIDUAL EVENTS

TABLE 1

COVERAGE OF SOLAR COSMIC RAYS

IN THE 19th SOLAR CYCLE

Dectector	Integral Intensity N(>10) (accuracy)	N(>30) (accuracy)	N(>100) (accuracy)	N(>1000) (accuracy)	Spectral Shape (accuracy)	Composition	Time dependence	Event Coverage
PCA	+100% - 50%	———	———	———	———	———	fair	Complete
Neutron Monitor	———	———	———	+100% - 50%	+100% - 50%	———	fair	Complete
Balloons & Rockets (i.e., G.T. Emulsions Scint. junctions)	———	———	±25%	±25%	± 50%	Some Coverage	incomplete	about 70% after 8/58
Satellites (i.e., G.T. Scint. junctions)	———	± 25%	———	———	± 50%	———	fair	complete in 1960 + 1961

TABLE 2

Element	Relative Flux
Hydrogen	1
Helium	1
Beryllium and Boron	$<2 \times 10^{-4}$
Carbon	5×10^{-3}
Nitrogen	1×10^{-3}
Oxygen	9×10^{-3}
Fluorine	$<3 \times 10^{-4}$
Neon	1×10^{-3}
Sodium through Argon	1×10^{-3}

TABLE 2. - Relative fluxes of various elements in solar cosmic rays for equal rigidity intervals.

TABLE 3

Date	t_R(>30 Mev): Hours	t_R(>100 Mev): Hours	t_D(>30 Mev): Hours	t_D(>100 Mev): Hours	N(>10 Mev): Protons/cm^2	N(>30 Mev): Protons/cm^2	N(>100 Mev): Protons/cm^2	P_o(Mv)	Composition (Proton to alpha ratio for a fixed energy) P/α	Ref.
2/23/56	6	3	30	16	1.8×10^9	1.0×10^9	3.5×10^8	195		(2)(20)(21)(22)
8/31/56			(36)			2.5×10^7	6×10^6	144		(2)
1/20/57			(24)			2×10^8	7×10^6	61		(2)
7/3/57			(30)			2×10^7				(23)(2)
8/9/57			(18)			1.5×10^6				(2)
8/29/57			(60)			1.2×10^8	3×10^6	56		(23)(2)
9/21/57			(24)			1.5×10^6				(2)
10/20/57			(30)			5×10^7	1×10^7	127		(2)
11/4/57			(18)			9×10^6				
2/9/58			(18)			1×10^7				(2)
3/23/58			40	20	2×10^9	2.5×10^8	1×10^7	64	1.0 ± 0.5	(2)(1)
4/10/58						5×10^6				(2)(1)
7/7/58			32	16	1.8×10^9	2.5×10^8	9×10^6	62		(2)(1)
8/16/58	10		18		4×10^8	4×10^7	1.6×10^6	64		(2)(1)
8/22/58	10	3	20	8	8×10^8	7×10^7	1.8×10^6	56		(2)(1)(23)

TABLE 3
p. 2

Date	t_R(>30 Mev): Hours	t_R(>100 Mev): Hours	t_D(>30 Mev): Hours	t_D(>100 Mev): Hours	N(>10 Mev): Protons/cm^2	N(>30 Mev): Protons/cm^2	N(>100 Mev): Protons/cm^2	P_o(Mv)	Composition (Proton to alpha ratio for a fixed energy) P/α	Ref.
8/26/58			12		1.5×10^9	1.1×10^8	2.0×10^6	51		(2)(1)
9/22/58			(30)		9×10^7	6×10^6	1×10^5	50		(2)
5/10/59	20	10	22	14	5.5×10^9	9.6×10^8	8.5×10^7	84	1.0 ± 0.5	(2)(1)(24)(7)
6/13/59		(24)				8.5×10^7				
7/10/59	30	18	40	20	4.5×10^9	1.0×10^9	1.4×10^8	104	2.2 ± 0.5	(2)(1)(25)
7/14/59	16	12	18	12	7.5×10^9	1.3×10^9	1.0×10^8	80	1.0 ± 0.5	(2)(1)(25)
7/16/59	12	4	30	18	3.3×10^9	9.1×10^8	1.3×10^8	105	1.0 ± 0.5	(2)(1)(25)(26)(27)(7)
8/18/59		(24)				1.8×10^6				
1/11/60	6		30			4×10^5				(28)
4/1/60	2-3	<1	6	4	1.5×10^7	5.0×10^6	8.5×10^5	116		(2)(1)(28)
4/5/60	3		12			1.1×10^6				(2)(1)(28)
4/28/60	3	2	8	5	1.3×10^7	5.0×10^6	7×10^5	104		(2)(1)(28)
4/29/60						7×10^6				(2)(1)(28)
5/4/60	2-3	1	14	6	1.2×10^7	6×10^6	1.2×10^6	127	≥ 50	(2)(1)(28)(29)(30)(31)
5/6/60	3		24			4×10^6				(2)(1)(28)
5/13/60	3		15		1.5×10^7	4×10^6	4.5×10^5	94		(2)(1)(28)

TABLE 3
p. 3

Date	t_R (>30 Mev): Hours	t_R (>100 Mev): Hours	t_D (>30 Mev): Hours	t_D (>100 Mev): Hours	N(>10 Mev): Protons/cm^2	N(>30 Mev): Protons/cm^2	N(>100 Mev): Protons/cm^2	P_o (MV)	Composition (Proton to alpha ratio for a fixed energy) P/α	Ref
6/1/60	2		20			4×10^5				(28)
8/12/60	10		50			6×10^5				(28)
9/3/60	12	6	32	26	9×10^7	3.5×10^7	7×10^6	127	≥40	(2)(28)(32)(33)(34)(16)(7)
9/26/60					2×10^7	2.0×10^6	1.2×10^5	73		
11/12/60	10	8	18	14	4×10^9	1.3×10^9	2.5×10^8	124	1.0 ± 0.5	(2)(28)(35)(36)(16)(17)(30)(18)
11/15/60	8	4	16	10	2.5×10^9	7.2×10^8	1.2×10^8	114	2 ± 1	(2)(28)(36)(30)(18)(7)
11/20/60	2	1	10	5	1.4×10^8	4.5×10^7	8×10^6	118		(2)(28)
7/11/61	8-10	4	22-26	18	1.7×10^7	3×10^6	2.4×10^5	81		(19)
7/12/61	8-12	6	16-20	12	5×10^8	4×10^7	1×10^6	56		(2)(19)(7)
7/18/61	6-10	2-3	24	12	1×10^9	3×10^8	4×10^7	102	6 ± 1	(2)(19)(7)
7/20/61	4-6	1.5	6-8	3	1.5×10^7	5×10^6	9×10^5	120		(19)
9/28/61	1.5	1	12	8	5×10^7	6×10^6	1.1×10^6	121		(1)

DISTRIBUTION LIST

NASA Headquarters

R. J. Allenby - SM
P. E. Culbertson - MTL
J. H. Disher - ML
F. P. Dixon - MTY
W. B. Foster - SM
E. Z. Gray - MT
J. K. Holcomb - MAO
T. A. Keegan - MA-2
J. W. Keller - RV-1
G. A. Lemke - MAR
D. R. Lord - MTX
S. C. Phillips - MA
M. J. Raffensperger - MTE
A. Reetz, Jr. - RV-1
L. Reiffel - MA
M. Savage - MAT
A. W. Schardt - SG
M. L. Seccomb - MAP
W. B. Taylor - MLA
J. H. Turnock - MA-4
NASA Hq. Library - ATSS-10

Manned Spacecraft Center

W. A. Lee - PA
J. Modisette - ET32
D. E. Robbins - ET32
J. F. Shea - PA
W. E. Stoney, Jr. - ET

Marshall Space Flight Center

R. D. Shelton - R-RP-N

Bellcomm

G. A. Brill
F. C. Childs
R. E. Gradle
J. A. Hornbeck
B. T. Howard
C. A. Lovell
J. Z. Menard
C. R. Moster
I. D. Nehama
I. M. Ross
T. H. Thompson
R. L. Wagner
All members, Division 101
Department 1023
Central File
Library